Structural and Optical Properties of Small Cadmium Selenide Nanocrystallites

by

Dean Philipp

B.A., Chemistry and Physics
University of Wisconsin-Madison, 1992

Submitted to the Department of Chemistry in Partial Fulfillment of the Requirements for the Degree of

Master of Science in Chemistry

at the
Massachusetts Institute of Technology
June, 1995

Signature of Author .....
Department of Chemistry
May 12, 1995

Certified by .....
Moungi G. Bawendi, Associate Professor of Chemistry
Department of Chemistry
Thesis Supervisor

Accepted by .....
Dietmar Seyferth
Chairman, Departmental Committee on Graduate Students

STRUCTURAL AND OPTICAL PROPERTIES OF SMALL
CADMIUM SELENIDE NANOCRYSTALLITES
by
DEAN PHILIPP

Submitted to the Department of Chemistry on May 12, 1995 in partial fulfillment of the requirements for the Degree of Master of Science in Chemistry

ABSTRACT

Tiny nanocrystallites of cadmium selenide of about 15 Å in diameter were synthesized in solution using organometallic precursors. These tiny nanocrystallites are produced as a nearly discrete species as evidenced by optical absorption spectra. Absorption spectra of these tiny clusters were taken in various solvents, with the spectra showing solvent effects on the absorption peak positions. Photoluminescence excitation (PLE) scans for the tiny clusters at both room temperature and low temperature (77 K) were monitored at various luminescent wavelengths, with the PLE scans showing discrete transitions having a temperature dependence analogous to the temperature dependence of the bulk band gap. The PLE scans also show significant absorption into surface states at room temperature. Fluorescence scans on the tiny clusters at both room temperature and 77 K were taken at various excitation wavelengths, showing that the luminescence is mainly from the deep-trap surface states, except for room temperature emission at higher energy excitation, where band-edge luminescence is prominent. Ordered films of the tiny nanocrystallites were prepared. X-ray powder diffraction and electron diffraction was performed on the films, and the ordering was found to be in a hexagonal system. Attempts at growing single crystals of the tiny clusters were made with no success to date.

Small nanocrystallites of cadmium selenide ranging in size from 24 Å to 41 Å in diameter were synthesized in solution at high temperature (380 °C) to yield particles having high crystallinity, very few stacking faults, and a narrow size distribution. XRD patterns of these particles as glassy films were collected, while XRD patterns for particles approximating these in size, shape, and structure were simulated. The {110}, {103}, and {112} reflection peaks of the simulated XRD patterns were analyzed by fitting to gaussians to show the difficulties involved with such attempts of extracting lattice constants from peak positions of XRD patterns for such nanocrystallites. Next, keeping in mind these pitfalls, the experimental XRD patterns were analyzed by fitting to gaussians as well, showing virtually no lattice contraction for the nanocrystallites. Finally, a better way of analysis for such small particles, fitting the experimental XRD patterns to the simulated patterns and allowing for variation in the lattice constant, was employed. This analysis found very small lattice contractions for the nanocrystallite, no greater than a few tenths of a percent.

Thesis Supervisor: Dr. Moungi G. Bawendi
Title: Associate Professor of Chemistry

This is dedicated to my parents, Virginia Lemkuil and Wayne Philipp.

Acknowledgments

I would like to thank my advisor Moungi Bawendi for allowing me to perform research in his group and for his guidance and support. I would also like to thank the members of my research group for their help, including Bashir Dabbousi, Cherie Kagan, Masaru (Ken) Kuno, Fred Mikulec, Chris Murray, Manoj Nirmal, David Norris, and Ann Sacra.

TABLE OF CONTENTS

LIST OF FIGURES

CHAPTER 1: STRUCTURAL AND OPTICAL PROPERTIES OF TINY CADMIUM SELENIDE NANOCRYSTALLITES

I. Introduction

Semiconductor nanocrystallites, including those of cadmium selenide, are currently the focus of much fascinating research, mainly because their small size results in properties between molecules and bulk crystals. The study of such clusters can therefore reveal the evolution of bulk properties. At the molecular-like end of the size scale are tiny cadmium selenide clusters which are only about 15 Å in diameter. Research involving such clusters is not only interesting because these clusters are the smallest nanocrystallites with a crystalline core, but also because these clusters can be made as a nearly discrete species and thus provide a unique opportunity for structural and optical characterization.

The method of synthesizing these tiny cadmium selenide clusters is based on a method described by Murray, et al.,[1] which is used to synthesize clusters ranging in size from about 20 to 120Å in diameter. These clusters are made through the mixing of organometallic precursors in a coordinating solvent, which prevents growth of the clusters and passivates the surface. For the larger nanocrystallites, the mixing is done at very high temperature to cause a discrete nucleation, and the resulting particles are grown to larger size through careful control of the temperature. The tiny clusters, however, result as a thermodynamic minimum after reaction at a much lower temperature.

Though the crystalline cores of resulting tiny clusters have the structure of bulk cadmium selenide, the optical properties have not yet evolved into those of the bulk due to their small size. Solid state physics has two extreme models for simply representing periodic structures. The first, the weak potential model, represents the electronic states as free electrons perturbed by a weak periodic potential, which is most applicable in the case of metals. This gives rise to continuous bands in the bulk separated by a band gap. The boundary conditions for nanocrystallites would then give rise to discrete states rather than a continuous band. The tight-binding method assumes that the electrons are held closely

by individual atoms (or molecules), but that there is significant overlap between neighbors. This results in several closely spaced states that form continuous bands in the bulk limit. This model is especially applicable for semiconductor materials with a high degree of covalency, such as cadmium selenide, and would additionally be applicable to the ordering of clusters in a superlattice.

II. Synthesis of Tiny Nanocrystallites

The tiny nanocrystallites are synthesized by a method similar to that described by Murray, et al.[1] A typical preparation of these clusters involves first drying and degassing about 20 g of trioctylphosphine oxide in the reaction flask by heating at about 160°C under vacuum for several hours. The contents of the flask are constantly stirred with a stir bar throughout the entire preparation. The temperature is then raised to about 200°C for about 20 minutes, after which the flask is filled with and maintained under argon. The temperature is then allowed to decrease to about 70 to 80°C, where it is stabilized. Meanwhile a solution is prepared in a dry box consisting of 10 ml of trioctylphosphine, 10 ml of a 1.0 M solution of trioctylphoshine selenide in trioctylphoshine, and 200 μl of dimethyl cadmium. This solution is thoroughly mixed and loaded into a 20 ml disposable syringe. The syringe is then quickly brought out of the dry box, and the solution within is immediately injected into the reaction flask through a rubber septum. The temperature of the resulting mixture is then brought back to and maintained in the range of 70 to 80°C. After several hours the mixture becomes a pale yellow color which eventually develops opaque swirls, probably due to clusters partially ordering in the solution and scattering light.

After this stage, the preparation of the clusters is complete. The reaction mixture is transferred to vials under inert conditions, either via cannula or through the use of a syringe, and stored in a dry box for later use. After cooling to room temperature, the reaction mixture becomes a paste of trioctylphosphine/trioctylphosphine oxide containing the clusters.

III. Absorption Spectra of Tiny Clusters in Various Solvents

The trioctylphoshine/trioctylphoshine oxide paste containing the clusters can be dispersed in several solvents such as alkanes, ethers, aromatics, and chlorinated solvents. Non-solvents of these tiny clusters include alcohols (long-chain alcohols such as octanol and decanol only very sparingly solvate the tiny clusters), acetonitrile, and *N,N*-dimethylformamide. The clusters can be purified by repeated dispersion in a solvent, precipitation by a non-solvent, and decanting to remove the resulting supernatant. A tiny amount of either trioctylphoshine or trioctylphoshine/trioctylphoshine oxide must be added during the dispersion step to guarantee the presence of enough capping group and prevent irreversible flocculation of the clusters. Excess cadmium and selenium can be removed (as well as irreversibly aggregated clusters) by filtration of the clusters in solution.

After purification, the tiny clusters can be dispersed in any solvent and the absorption spectrum for the solution can be collected. This was done at room temperature for the clusters in solutions of nonane, toluene, chloroform, tetrahydrofuran, and diethyl ether using a Hewlett-Packard 8452 diode array spectrometer. The resulting absorption spectra can be observed in Figure 1-1 (page 12), where absorbance of the tiny clusters in the various solvents versus wavelength is shown. The discrete energy states for these tiny clusters are immediately visible in these spectra, with the extreme narrowness of the linewidths for these tiny clusters being especially noticeable. The first absorption feature in these spectra occurs at a wavelength around 410 nm and varies in position and shape, as well as the other absorption features, for the various solvents. This indicates that there must be some interesting effects on the energy states due to solvent interactions with the capping groups and/or surface atoms. Polarization of the clusters by the solvent could be one possible interaction, with the resulting effects on the spectra being the shifting of non-polar states to lower energy (larger wavelength) and the broadening of polar states. This could not be the only factor, if it is indeed a major factor, since the spectrum in tetrahydrofuran, which is a more highly polar solvent that diethyl ether, does not yield the expected results when compared to the spectrum in diethyl ether.

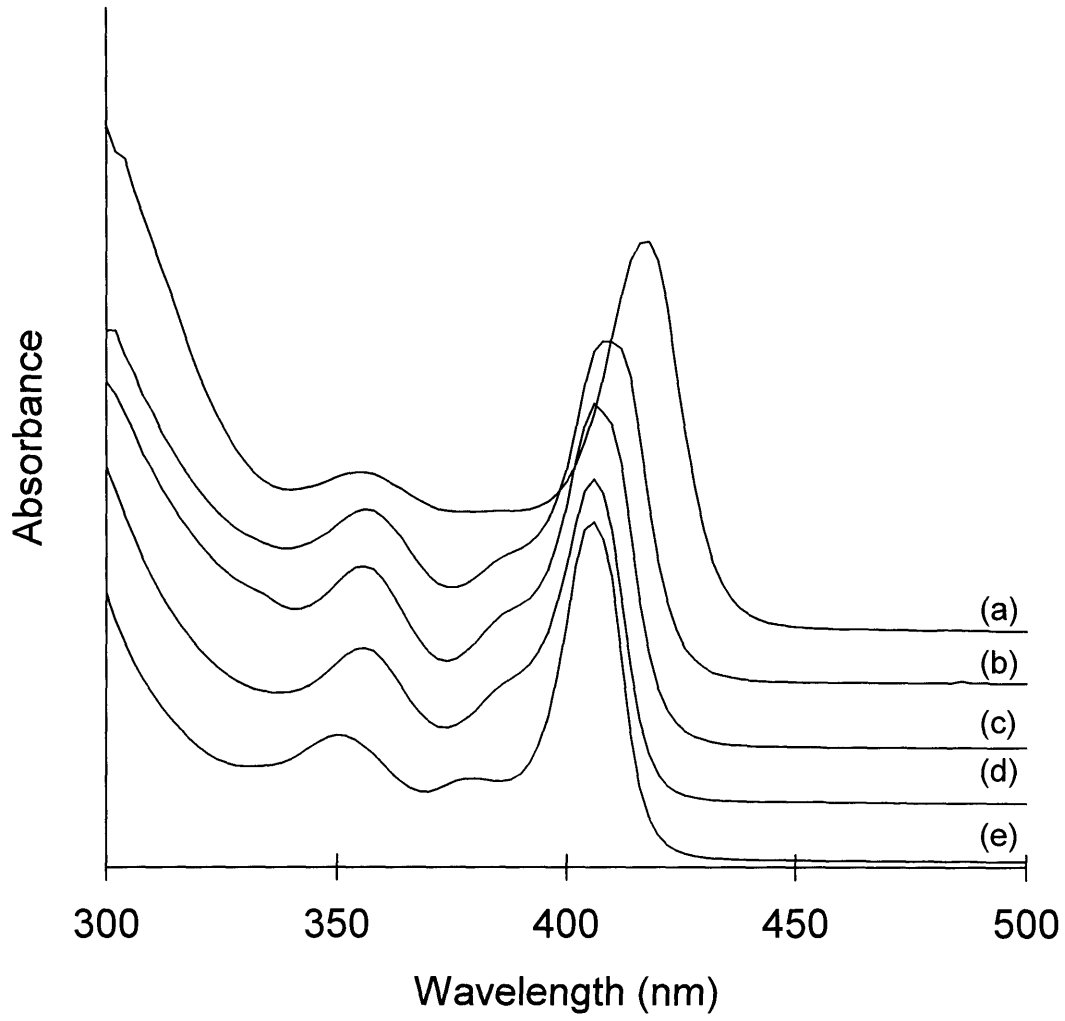

Figure 1-1. Absorption spectra for tiny CdSe nanocrystallites in various solvents: (a) diethyl ether, (b) nonane, (c) toluene, (d) chloroform, (e) tetrahydrofuran.

IV. Photoluminescence Excitation and Fluorescence for the Tiny Clusters

Photoluminescence excitation (PLE) scans can be performed for the tiny clusters in the trioctylphoshine/trioctylphoshine oxide paste by illuminating the clusters in paste, scanning through wavelengths of this exciting light, and collecting the emission at a given wavelength as a function of the wavelength of the exciting light. PLE scans are thus similar to absorption spectra in the information that they provide, however one key difference is that absorption spectra probe excitation into energy states, while PLE scans only probe excitation into states for which emission eventually occurs at a given wavelength. PLE scans with the tiny clusters were collected at various emission wavelengths at both room temperature and at liquid nitrogen temperature (77 K), and can be seen in Figures 1-2a and 1-2b (page 14). The PLE scans were carried out on a SPEX Fluorolog-2 spectrometer using front face collection. The slit sizes used were 1.0 mm at room temperature and 0.5 mm at 77 K. Comparing the scans at room temperature in Figure 1-2a with those at 77 K in Figure 1-2b, a temperature dependence analogous to the temperature dependence of the bulk band gap[2] can be seen. It must also be noted that the amplitudes of the scans at 77 K are much larger than those of the scans at room temperature, indicating a much greater quantum yield at lower temperatures. Also apparent from these scans is the significant absorption into surface sates at room temperature.

Fluorescence scans can be performed by illuminating the clusters in paste at a given wavelength and scanning through the emission wavelength, collecting the emission along the way as a function of the emission wavelength. Fluorescence scans with the tiny clusters were collected for various excitation wavelengths at both room temperature and at 77 K, and can be seen in Figures 1-3a and 1-3b (page 15). The fluorescence scans were also carried out on a SPEX Fluorolog-2 spectrometer using front face collection, with slit sizes of 1.0 mm at room temperature and 0.5 mm at 77 K. Evident from the figures is that the luminescence is mainly from deep-trap surface states, except for room temperature emission for higher energy excitation, where band-edge luminescence is prominent.

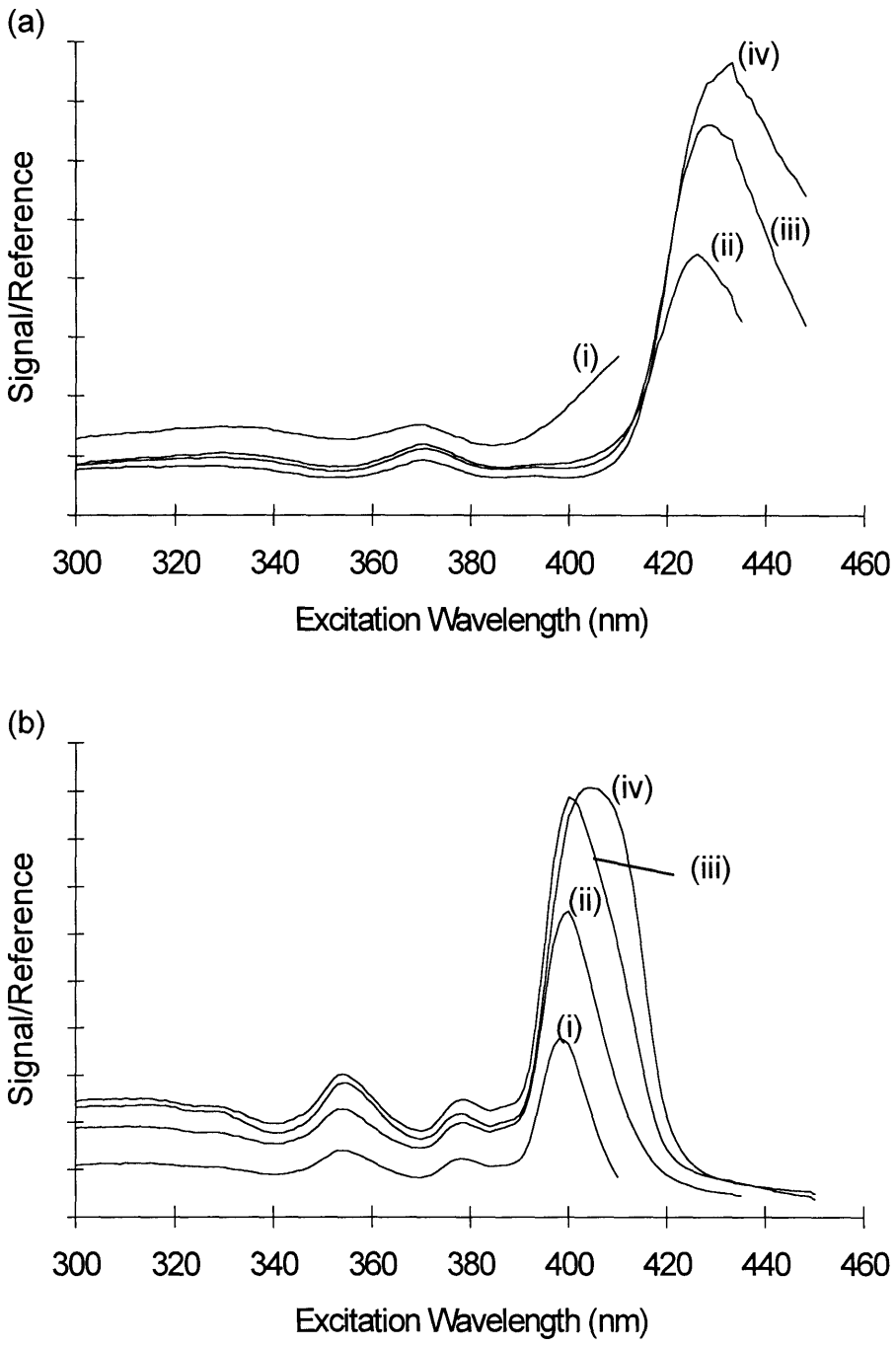

Figure 1-2. Photoluminescence excitation scans of tiny CdSe nanocrystallites at (a) room temperature and at (b) 77 K. The emission wavelengths for the scans are: (i) 425 nm, (ii) 450 nm, (iii) 470 nm, and (iv) 500 nm.

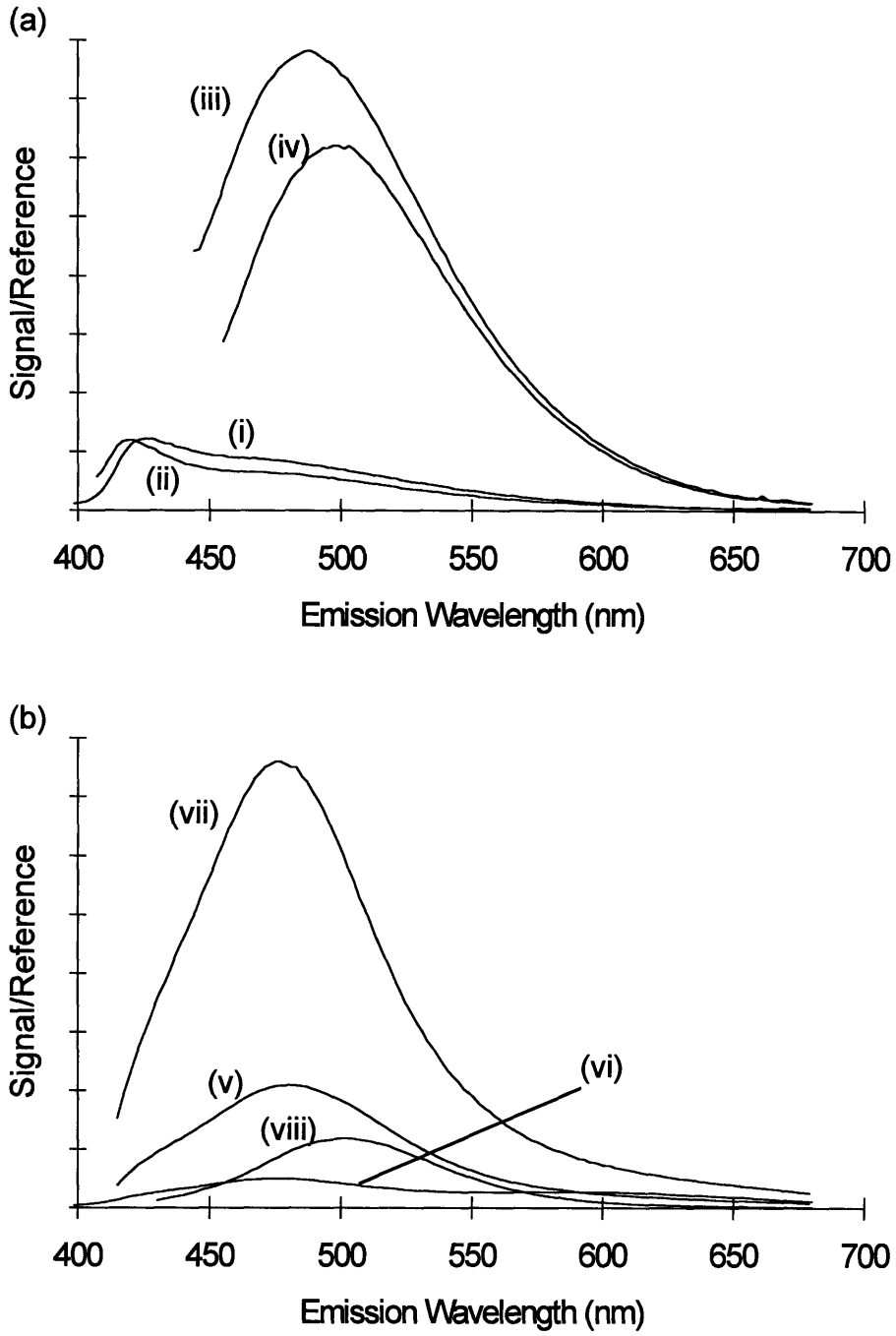

Figure 1-3. Fluorescence scans of tiny CdSe nanocrystallites at (a) room temperature and at (b) 77 K. The excitation wavelengths for the scans in (a) are: (i) 370 nm, (ii) 392 nm, (iii) 427 nm, and (iv) 440 nm. The excitation wavelengths for the scans in (b) are: (v) 355 nm, (vi) 379 nm, (vii) 400 nm, and (viii) 415 nm.

V. Ordered Films of the Tiny Clusters

Highly ordered films of the tiny clusters were prepared by first purifying the clusters using the procedure described above with chloroform as the solvent and acetonitrile as the non-solvent. The dispersion/precipitation/decanting sequence was repeated three times before final dispersion in nonane. This solution of clusters in nonane was then filtered and concentrated by removal of solvent under vacuum. To this concentrated solution (about 0.2 ml) was added a drop or two of octanol. Ordered films for x-ray powder diffraction studies were the formed by carefully dropping a couple drops of the solution onto a Si (001) wafer and allowing to dry completely, while films for electron diffraction studies were prepared by brushing a copper grid against a drop of the solution and allowing to dry completely. The copper grids were from Ernest Fullam and were 300 mesh with an approximately 50 Å coating of amorphous carbon. It must be noted that all steps in making the films were carried out under an inert atmosphere.

The structure of the resulting films was first characterized through powder x-ray diffraction (XRD). XRD patterns were collected on a Rigaku 300 Rotaflex diffractometer operating in the Bragg configuration using Cu K_α radiation. The accelerating voltage was set at 50 KV with a 200 mA flux. Divergence and scatter slits of ½° were used along with a 0.15° receiving slit. The pattern obtained for one of the prepared films can be seen in Figure 1-4a (page 17) where the log of the scattered intensity is plotted as a function of 2θ. The assignment of peaks is that of a hexagonal system. The progression of sharp peaks shows a highly ordered structure, while the predominance of the peaks in this progression over any other peaks indicates a preferred orientation. Also supportive of a preferred orientation is the fact that the intensity of the {110} reflection peak varies relative to the intensity of the peaks in the progression. The relative intensities of the peaks in the progression appears to be due to the shape of the individual particles themselves. Shown in Figure 1-4b (page 17) are the theoretical form factors for simulated clusters. Plot (i) shows the log of the scattered intensity for a simulated spherical cluster with a diameter of 12 Å while plot (ii) shows the log of the scattered intensity for a simulated cluster with the idealized structure of that found by Herron, et

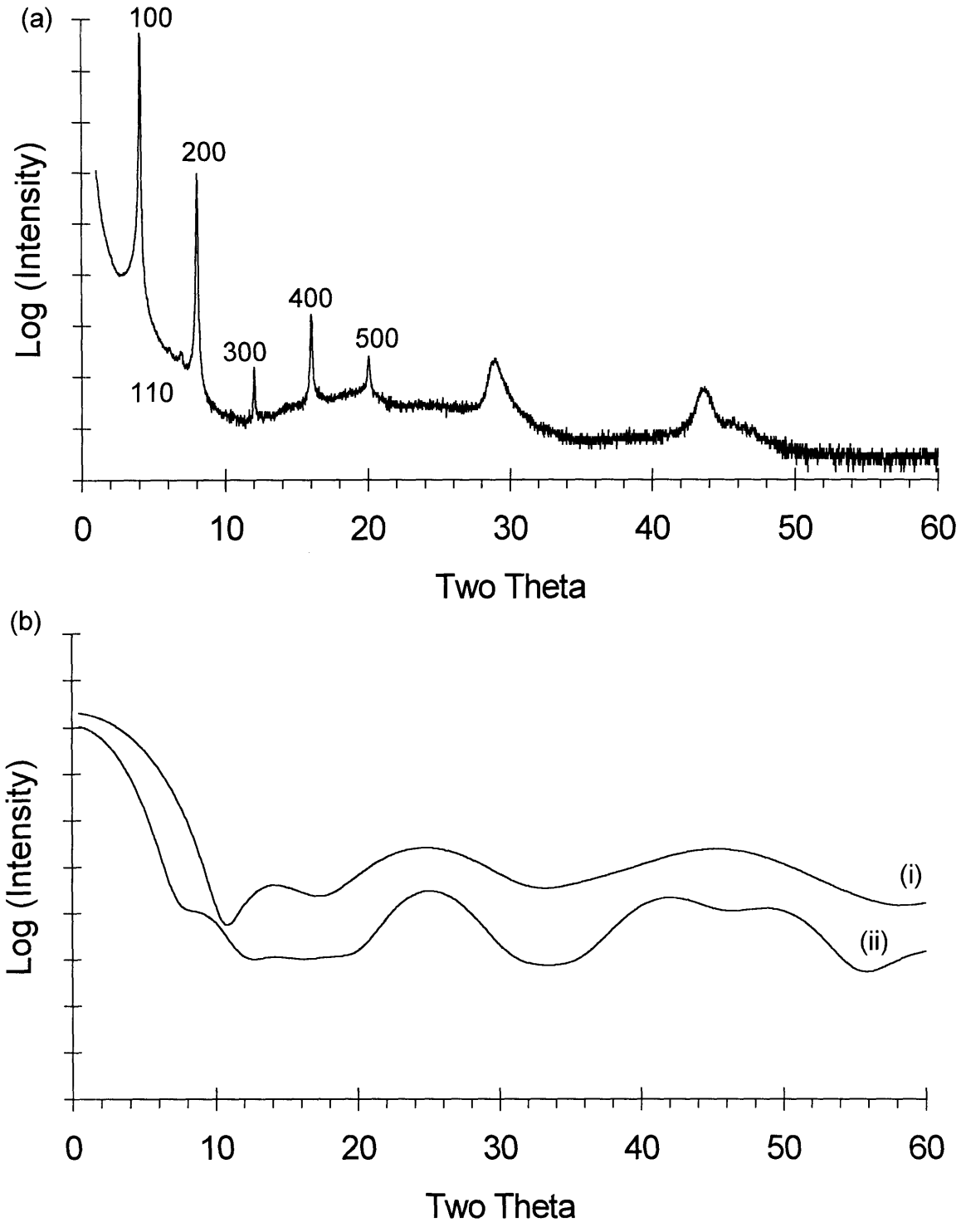

Figure 1-4. X-ray diffraction powder patterns for an ordered film of tiny CdSe nanocrystallites, with (a) showing the experimental pattern and (b) showing theoretical form factors for the tiny clusters. In (b), curve (i) is for spherical clusters about 12 A in diameter while curve (ii) is for tetrahedral clusters having an idealized structure.

al.[3] for CdS, but substituting the bulk lattice constant of CdSe of a = 4.2999 Å.[4] The intensity of the peaks in the progression generally follow the form factor curves for values of 2θ up to about 20°, which is the portion of the form factor due to the shape and size of the particles. Scattering above this region would be due to the internal crystal structure of the particles themselves, and would be present in the pattern for the ordered clusters only if there was an exact relation between the internal crystal structure of neighboring clusters. Therefore reasons for the discontinuation of the progression above {500} could include that the particles could not be perfectly aligned with respect to one another and that there is some static disorder between clusters in the ordered film. Explanations for the presence of broader peaks at larger angles currently remains a mystery.

The ordered films were also characterized using electron diffraction, which was done using a JEOL 200 CX transmission electron microscope operating at 200 kV. Figures 1-5a and 1-5b (page 19) show electron diffraction patterns obtained for an ordered film of clusters prepared on a carbon coated copper grid. In Figure 1-5a, selected area diffraction is used to probe a very small area of the film using a camera length of 330 cm. Apparent from this pattern is the hexagonal structure of the film, as the rings show spots in a hexagonal array due to a highly ordered domain. Because the rings are too closely spaced at this camera length, Figure 1-5b shows a diffraction pattern for a camera length of 15 m. To achieve this large of a camera length, the high dispersion mode had to be used which probed a much larger area. Because a large number of ordered domains is now being probed, the rings appear nearly continuous.

VI. Attempts to Crystallize the Tiny Nanocrystallites

Though preparation of ordered films of the tiny nanocrystallites was successful, growing single crystals of these clusters had not been successful. However, many attempts at such crystal growth were attempted. The methods tried were various recrystallization techniques, both with and without added non-solvent, and techniques of slowly approaching saturation of the clusters in solution by the gradual addition of non-solvent. The recrystallization attempts involved first purifying the clusters using the

(a)

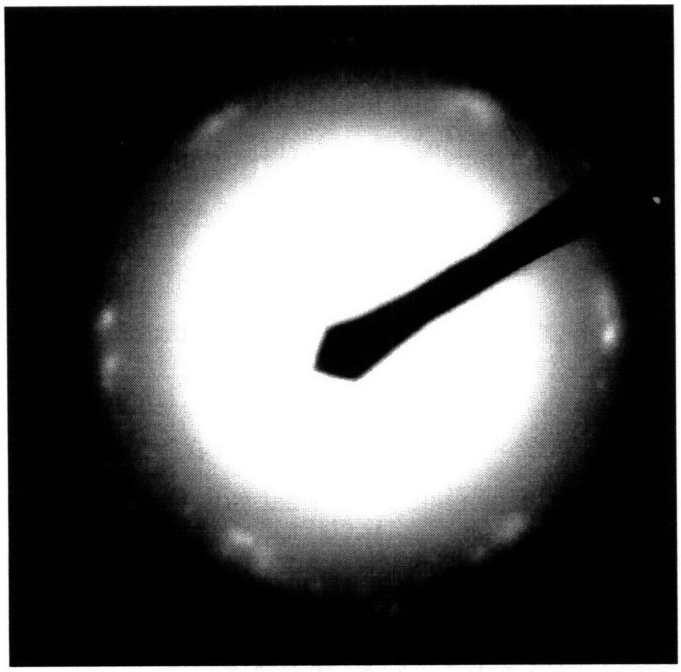

(b)

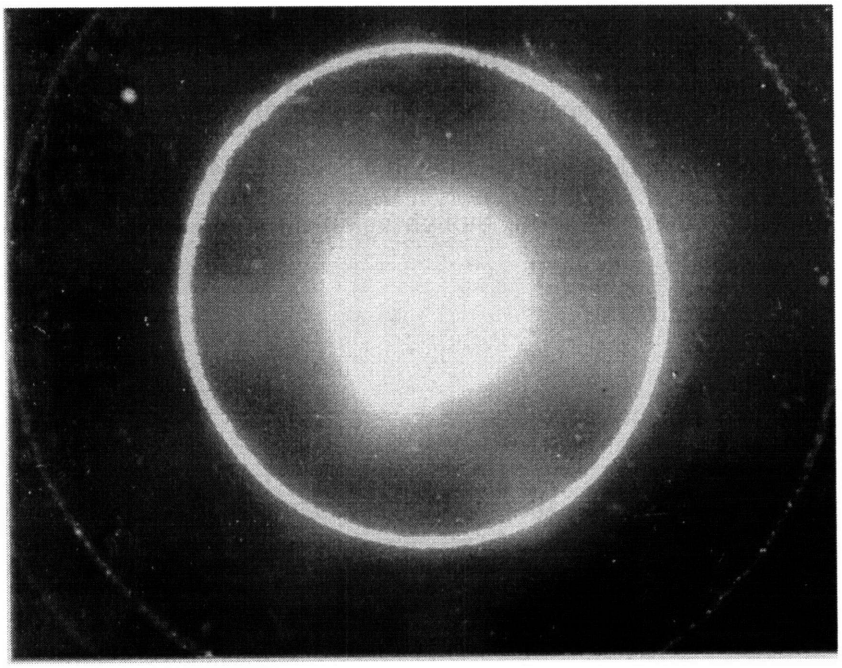

Figure 1-5. Electron diffraction patterns of ordered films of tiny CdSe nanocrystallites. (a) Selected area diffraction pattern, camera length = 330 cm. (b) High dispersion diffraction pattern, camera length = 15 m.

procedure described above in the preparation of ordered films and dispersing the clusters in a final solvent such as nonane, chloroform, tetrahydrofuran, toluene, or hexane. At this point, small amounts of non-solvents such as methanol, acetonitrile, *N,N*-dimethylformamide, or octanol may be added in varying concentrations. The resulting solutions with or without added non-solvent were then stored in darkness either in an isolated cabinet or in a freezer for up to several months. To date, these attempts have shown no signs of forming singe crystals and have only formed flocculates or remained as solutions.

The attempts to slowly saturate the clusters with non-solvent again involved first purifying the clusters and dispersing in a final solvent. One technique of slowly saturating the clusters was, depending upon the density of the solvent relative to the desired non-solvent, to either add the solution of clusters to a vial and very carefully adding a non-solvent as a layer above the solution phase or doing the reverse with the solution phase over the non-solvent. The gradual saturation was the result of the diffusion of non-solvent into the solution phase, though only flocculation occurred. A second technique was to add the solution to one side of an H-cell, adding non-solvent to the other side, and storing the sealed H-cell in a dark, isolated cabinet for up to several months. The saturation was accomplished by the gradual evaporation and diffusion of the non-solvent into the cluster solution, though again no signs of the formation of single crystals occurred, only flocculation.

VII. Conclusion

Tiny nanocrystallites of CdSe were synthesized as a nearly discrete species, as evident from absorption spectra of the clusters in various solvents. Also shown by these absorption spectra are solvent effects on the absorption peak positions. PLE scans of the clusters at both room temperature and at 77 K show discrete transitions having a temperature dependence analogous to that of the bulk band gap and show significant absorption into surface states at room temperature. Fluorescence scans of the clusters at both room temperature and 77 K show that the luminescence is mainly from deep-trap

states, except for room temperature emission for higher excitation energies, where band-edge luminescence is prominent. Ordered films of the tiny nanocrystallites were successfully prepared, though attempts at forming single crystals of the clusters have not been successful to date. The films, however, are ordered in a hexagonal system as evident from XRD and electron diffraction.

References

(1) Murray, C. B.; Norris, D. J.; Bawendi, M. G. *J. Am. Chem. Soc.* **1993**, *115*, 8706.

(2) Fan, H. Y. *Phys. Rev.* **1951**, *82*, 900.

(3) Herron, N.; Calabrese, J. C.; Farneth, W. E.; Wang, Y. *Science* **1993**, *259*, 1426.

(4) Reeber, R. R. *"J. Mat. Sci.* **1976**, *11*, 590.

CHAPTER 2: LATTICE CONTRACTIONS FOR SMALLER CADMIUM SELENIDE NANOCRYSTALLITES

I. Introduction

Recently there has been much interest in semiconductor nanocrystallites since such particles express properties between those of molecules and those of the bulk. These nanocrystallites have crystalline cores with a large fraction of atoms on the surface. Though several different methods have been developed to synthesize semiconductor nanocrystallites,[1-3] few research groups have been successful at producing identical particles capable of complete structural determination.[4-6] Therefore for virtually all of the particles only limited structural information is obtainable by such methods as powder x-ray diffraction (XRD), electron microscopy, and EXAFS.

One unanswered question pertaining to the structure of semiconductor nanocrystallites is whether or not there is a lattice contraction from that of the bulk. Several groups have found lattice contractions for metal clusters,[7-11] typically on the order of a few percent of that for the bulk. Metal bonding, however, is isotropic, while that of semiconductors is quite directional due to a high degree of covalency. Nevertheless, some researchers expect to see a lattice contraction in semiconductors as well, often citing arguments based on simple models of surface tension. So far, though, EXAFS data for cadmium chalcogenide nanocrystallites indicate contractions in nearest-neighbor bond lengths of no more than 1%,[12] and even in the exact structure found by Herron, et al. for $Cd_{32}S_{14}(SC_6H_5)_{36}\cdot DMF_4$ bond contractions of only about 0.5% are present in the core.[4] It may be noted that EXAFS methods probe the average bond lengths throughout the particles while XRD probes distances between planes in the crystalline core of the particles. This paper relates the use of XRD techniques on CdSe nanocrystallites in attempting to shed more light on any possible contractions in semiconductor nanocrystallites. First, difficulties involved with such attempts will be explored by simulating XRD patterns for the nanocrystallites and analyzing them by fitting to gaussians. Next, keeping in mind the pitfalls, experimental XRD patterns for CdSe

nanocrystallites will be analyzed by fitting to gaussians. Finally, a better way of analysis for such small particles, fitting to simulated patterns, will be used to analyze the experimental patterns.

II. Experimental

Semiconductor nanocrystallites of CdSe ranging in size from about 24 Å to 41 Å in diameter were prepared by the method of Murray, et al.[13] with some modifications to produce clusters with fewer stacking faults. These modifications included using a smaller, varying amount of trioctylphosphine in the injection along with varying the concentrations of dimethylcadmium and trioctylphosphine selenide present in the injection mixture. The actual amounts used were varied to control the size of particles produced and typically consisted of between 2.5 and 6.0 ml trioctyphosphine, between 10 and 30 μl dimethylcadmium, and enough trioctylphosphine selenide for a concentration four times that of the cadmium. This resulting mixture was then injected into 10g trioctylphosphine oxide at 380°C instead of at 300°C. Size selection on these particles did not have the dramatic effect that it for the particles made by Murray, et al. without modifications, though it did yield a narrow distribution with few particles absorbing far to the blue or far to the red of the peak absorption. Sizes of the particles were determined using a size versus peak absorption curve.[13]

XRD patterns were collected on a Rigaku 300 Rotaflex powder diffractometer operating in the Bragg configuration using Cu K_α radiation. The accelerating voltage was set at 60 kV with a 300 mA flux. Divergence and scatter slits of 0.5° were used along with a 0.3° receiving slit for nanocrystallite samples while divergence and scatter slits of ⅙° with a 0.15° receiving slit were used for bulk CdSe. The diffractometer was calibrated in the desired range of 38° to 54° using a quartz standard. Samples for XRD were prepared by dropping size selected particles dispersed in hexane on a Si (001) wafer and allowing the hexane to evaporate leaving the particles in a glassy form. For the determination of the lattice constants of bulk CdSe, a suspension of CdSe powder

(99.999%, -325 mesh, purchased from Alfa) in methanol was deposited on a Si (001) wafer to produce a very thin film.

III. Theory and Analysis

A. Simulations of XRD Patterns

To determine simulations of XRD patterns for the CdSe nanocrystallites, a crystallite of a given size, shape, and stacking sequence in the c direction was first constructed.[14] Interatomic distances between the atoms of different types (Cd-Cd, Se-Se, and Cd-Se) were calculated and binned into discrete distances. An algorithm using a discrete form of the Debye equation[15] was then employed. In this equation, the diffracted intensity is given by:

$$I(S) = \frac{I_0}{2\pi S} \sum_{i,j=Cd,Se} f_i(S) f_j(S) \sum_m \frac{p_m^{i,j}}{r_m} \sin(2\pi r_m S),$$

where I_0 is the incident intensity, $f_i(S)$ and $f_j(S)$ are the atomic scattering factors for Cd and Se, S is the scattering parameter [$S=2\sin(\theta)/\lambda$] for x-rays of wavelength λ diffracted through the angle θ, r_m is the m-th discrete interatomic distance, and $p_m^{i,j}$ is the frequency of r_m for a given combination of atom types i and j. The algorithm next involves finding fast sine transforms,[16] $J^{i,j}(S_l)$, of the function $(\frac{p_m^{i,j}}{r_m})$ for the discrete points S_l in reciprocal space. Finally, the Sampling theorem[17] is used to interpolate between the $J^{i,j}(S_l)$ to find $I(S)$ for a given value of 2θ:

$$I(S) = \frac{I_0}{\pi S} \sum_{i,j=Cd,Se} f_i(S) f_j(S) \sum_{m=-X}^{X} J^{i,j}(S_{l+m}) \frac{\sin[2\pi N \Delta r(S - S_{l+m})]}{2\pi N \Delta r(S - S_{l+m})},$$

where X is the smallest integer required for convergence within a desired precision, N is the number of discrete points in reciprocal space, and Δr is the increment between interatomic distances. N is related to the number M of the maximum interatomic distance, $r_M = M\Delta r$, by:

$$N = 2^n, \quad n = \mathrm{INT}[\log_2(2M)] + 1 .$$

This approach has the advantage in that it does not assume anything about the positions and widths of the peaks and thus accurately reproduces the convolutions of peaks resulting from the finite size and defect broadening of the particles. Thermal effects are included in the simulations by the introduction of a Debye-Waller factor[18] based on an average root-mean-square displacement of 0.2Å. Unfortunately, not enough is known about the samples to simulate the background scattering, so a linear model for the background in the experimental patterns was used.

B. Analysis - General Aspects

All methods of analyses involved non-linear fitting techniques using a χ^2 figure of merit:[16]

$$\chi^2 = \sum_{i=1}^{N} \frac{[f(x_i, \vec{a}) - y_i]^2}{\sigma_i^2},$$

where N is the number of data points (x_i, y_i), each with an associated uncertainty σ_i, and f is the modeling function with modeling parameter vector $\vec{a}$. The figure of merit χ^2 is minimized by varying the parameter vector $\vec{a}$ to achieve the best fit of the data to the modeling function.

C. Analysis by Fitting to Gaussians

For fitting simulations in the range of $x = 2\theta = 40°$ to $50°$ to three gaussians in order to model the {110}, {103}, and {112} peaks, the modeling function used was:

$$f(x_i, \vec{a}) = \sum_{j=0}^{2} a_{3j}\, \mathrm{e}^{-\left(\frac{x_i - a_{3j+1}}{a_{3j+2}}\right)^2},$$

while the modeling function for fitting experimental XRD patterns in the same range to three gaussians was:

$$f(x_i,\vec{a}) = \sum_{j=0}^{2} a_{3j}\, e^{-(\frac{x_i - a_{3j+1}}{a_{3j+2}})^2} - a_9 \cdot x_i + a_{10}\ .$$

All parameters a_i of the parameter vector $\vec{a}$ are positive, with a_9 and a_{10} representing respectively the (negative) slope and the constant comprising the linear background used in modeling the experimental patterns.

D. Analysis by Fitting to Simulations

For fitting experimental patterns to a combination of simulations plus a linear background, the modeling function used was:

$$f(x_i,\vec{a}) = \sum_{j=0}^{n-1} a_j I_j[x'(x_i,a_n)] \quad - a_{n+1} \cdot x_i + a_{n+2}; \quad x'(x_i,a_n) = 2\sin^{-1}[a_n \sin(\frac{x_i}{2})],$$

where n is the number of simulations I_j, each with amplitude a_j, used in the fit and a_{n+1} and a_{n+2} are respectively the (negative) slope and constant comprising the linear background. The function x' is used to shift the x-axis (2θ-axis) as a result of a change in the ratio a_n of the experimental lattice constant to the bulk value. The actual fits done involved only two simulations (n = 2), where I_1 and I_2 were simulations for pure wurtzite particles and for particles with a stacking arrangement of ...BABACAC... .

E. Estimations of Uncertainties

Uncertainties in the fitting parameters $\vec{a}$ were estimated in two ways. The first way involved just using the square roots of the diagonal elements of the covariance matrix C to find the uncertainties as $\Delta a_j = \sqrt{C_{jj}}$.[16] Because these elements relied upon the entered measurement errors $\sigma_i = \sigma^{exp}$, the second method first calculated errors in the measurements by the following:

$$\sigma^{calc} = \sqrt{\frac{\sum_{i=1}^{N}[f(x_i,\vec{a}) - y_i]^2}{N-m}} = \sigma^{exp}\sqrt{\frac{\chi^2}{N-m}},$$

where N is the number of data points and m is the number of parameters in $\bar{a}$, thus yielding $N-m$ as the degrees of freedom. Then, since the covariance matrix is proportional to $1/(\sigma^{exp})^2$, the uncertainties in the fitting parameters are just:

$$\Delta a_j = \sqrt{C_{jj}} \cdot \sqrt{\frac{\chi^2}{N-m}}.$$

In a successful model, these two methods would ideally yield the same values, though for these analyses, the larger of the two was the one actually used. For the analyses fitting gaussians to peaks, the uncertainties Δa_j were then propagated throughout subsequent calculations to produce estimates of uncertainties in the percent change from the bulk for each of the three peak centers and then an estimate of the uncertainty in the average percent change from the bulk. This last uncertainty, however, was compared to the standard deviation for the three percent changes in the average, with the charted uncertainty being the larger of the two. For the analyses fitting simulations to XRD patterns, the uncertainty in the parameter corresponding to the ratio of the experimental lattice constant to that of the bulk was just converted to the uncertainty in the percent change from the bulk, though this uncertainty was inherently quite large.

IV. Results and Discussion

A. Reasons for the Expectation of a Lattice Contraction

As mentioned in the introduction, surface tension arguments have been used in anticipation of lattice contractions in semiconductor nanocrystallites. In these arguments, the particles are likened to spherical liquid drops where a Laplace pressure $\Delta p = 2\gamma/r$ causes the following contraction:[19]

$$\frac{\Delta a}{a} = -\frac{2}{3}\frac{\gamma\kappa}{r}.$$

Here a and Δa are respectively the lattice constant and change in lattice constant, γ is the surface tension, κ is the isothermal compressibility, and r is the radius. Such an equation shows a linear relationship between the percent change from the bulk of the lattice

constant and the inverse of the radius. This is why the results of the analyses below were presented as plots of percent change from the bulk vs. 1/radius. Such plots, given κ, would in principle yield γ, though the large uncertainties make such a determination unreliable. This simple model of surface tension does assume that the Laplace pressure is felt isotropically throughout the particle and therefore neglects any possibility that the pressure may be felt mainly by the atoms at or near the surface. Thus just one possible explanation for the measured lattice contractions to be smaller in magnitude than one may expect could be due to reconstruction occurring mainly at or near the surface, which is indeed the case for the $Cd_{32}S_{14}(SC_6H_5)_{36}\cdot DMF_4$ cluster of Herron, et al.[4]

B. Discussion on Choice of XRD Region Analyzed

For all analyses of XRD patterns, simulated and experimental, the portion of the patterns used was that between $2\theta=40°$ to 52°, which is mainly made up of the {110}, {103}, and {112} wurtzite reflections. The reasons for choosing this portion are so that three strong peaks instead of one could be used for the analyses, with the three peaks being closely spaced and thus minimizing effects from the background difficult for which to compensate. The "peak" around $2\theta=25°$ was expressly chosen against since it really is the convolution of three very closely spaced peaks, {100}, {002}, and {101}, and as demonstrated in Reference 13, is highly susceptible to shifts due to a change in shape.

C. Difficulties in Analysis Due to Shape and Defects

As stated above, simulations of the XRD patterns can accurately include effects due to the small size, shape, and defects of nanocrystallites. Therefore, to point out the difficulties associated with analysis of the directly observed peaks, XRD patterns were simulated for nanocrystallites about 30Å in diameter and analyzed by fitting to three gaussians. The simulations used were for 30Å particles having a pure wurtzite arrangement, an arrangement with a stacking fault at the center (...BAB<u>A</u>CAC..., where A,B,C designate planes in the c direction and the underline designates the central plane),

and an arrangement with a stacking fault slightly further from the center (...BAB<u>A</u>BCB...) and for ellipsoidal particles 29Å x 31Å (the axis in the c direction was 15.5Å while the axis in the radial direction was 14.5Å) having the same three planar sequences. The results are shown in Figure 2-1 (page 31), where Figure 2-1a shows the percent change of the lattice constant from that of the bulk for each of the individual peaks and Figure 2-1b shows the percent change of the lattice constants from the bulk for the average of the three peaks. The determined lattice constants for bulk CdSe were a = 4.2979±0.0002Å and c = 7.0075±0.0006Å, which compare relatively well with previously published values of a = 4.2999±0.0003Å and c = 7.0109±0.0005Å.[20] As can be seen in Figure 2-1a, changing the stacking arrangement can cause significant shifts in the positions of the individual peaks, as there is much change in the shift for any given reflection amongst both groups (i), (ii), (iii) and (iv), (v), (vi), where (i) and (iv) are for pure wurtzite, (ii) and (v) are for a stacking fault at the center, and (iii) and (vi) are for a stacking fault slightly further from the center. Also, changing the shape from spherical [(i), (ii), (iii)] to just slightly ellipsoidal [(iv), (v), (vi)] causes shifts. Perhaps most notable in Figure 2-1a is that there can be significant scatter between peaks of the same pattern. These shifts for the different peaks are not completely independent, as can be seen in Figure 2-1b where the average shifts are not nearly as erratic, though there still is some variation. These charts demonstrate that different shape and defects can have significant effects on the shifts from the bulk, leading to obvious difficulties when dealing with particles that have ambiguous shapes and stacking arrangements.

D. Difficulties in Analysis Due to Small Size

Next, simulations for two series of particles with varying sizes, one series of pure wurtzite and one with the stacking arrangement ...BAB<u>A</u>CAC..., were fit with gaussians. A plot of the average percent change from the bulk for the three peaks versus size for both series can be seen as Figure 2-2 (page 32). Apparent in Figure 2-2 is a trend of the percent changes becoming larger, corresponding to shifts towards lower angles, as size is decreased. Thus a slight lattice dilation is falsely indicated. This trend is present in both

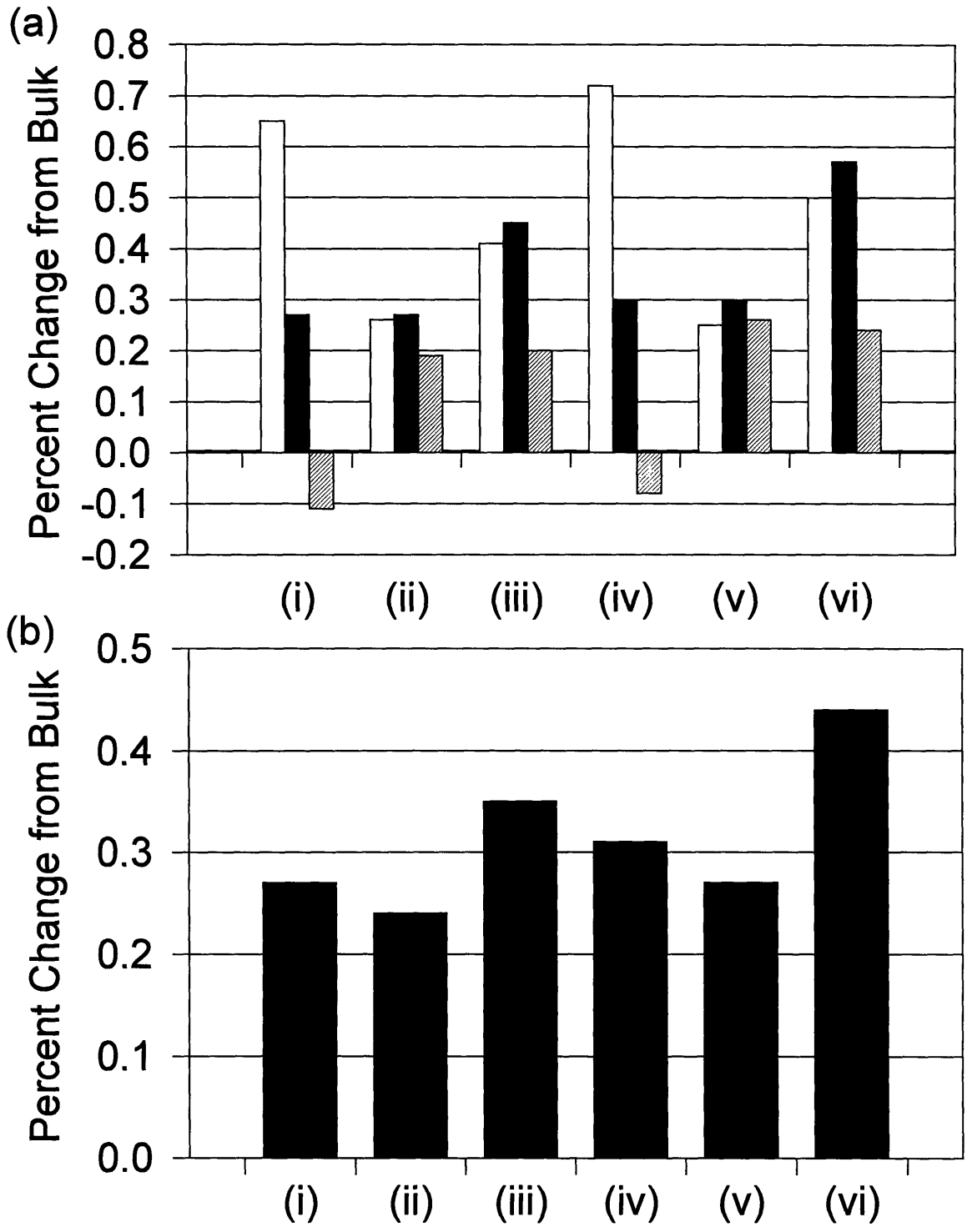

Figure 2-1. Results of fitting gaussians to simualtions of various particles approximately 30Å in diameter. (a) Percent change from the bulk for each of the three gaussians:□ {110},■ {103},▨ {112}. (b) Average percent change from the bulk for the three gaussians. The particles simulated were: (i) 30Å dia., wurtzite; (ii) 30Å, ...BAB$\underline{A}$CAC...; (iii) 30Å, ...BAB$\underline{A}$BCB...; (iv) 29Å x 31Å, wurtzite; (v) 29Å x 31Å, ...BAB$\underline{A}$CAC...; and (vi) 29Å x 31Å, ...BAB$\underline{A}$BCB... .

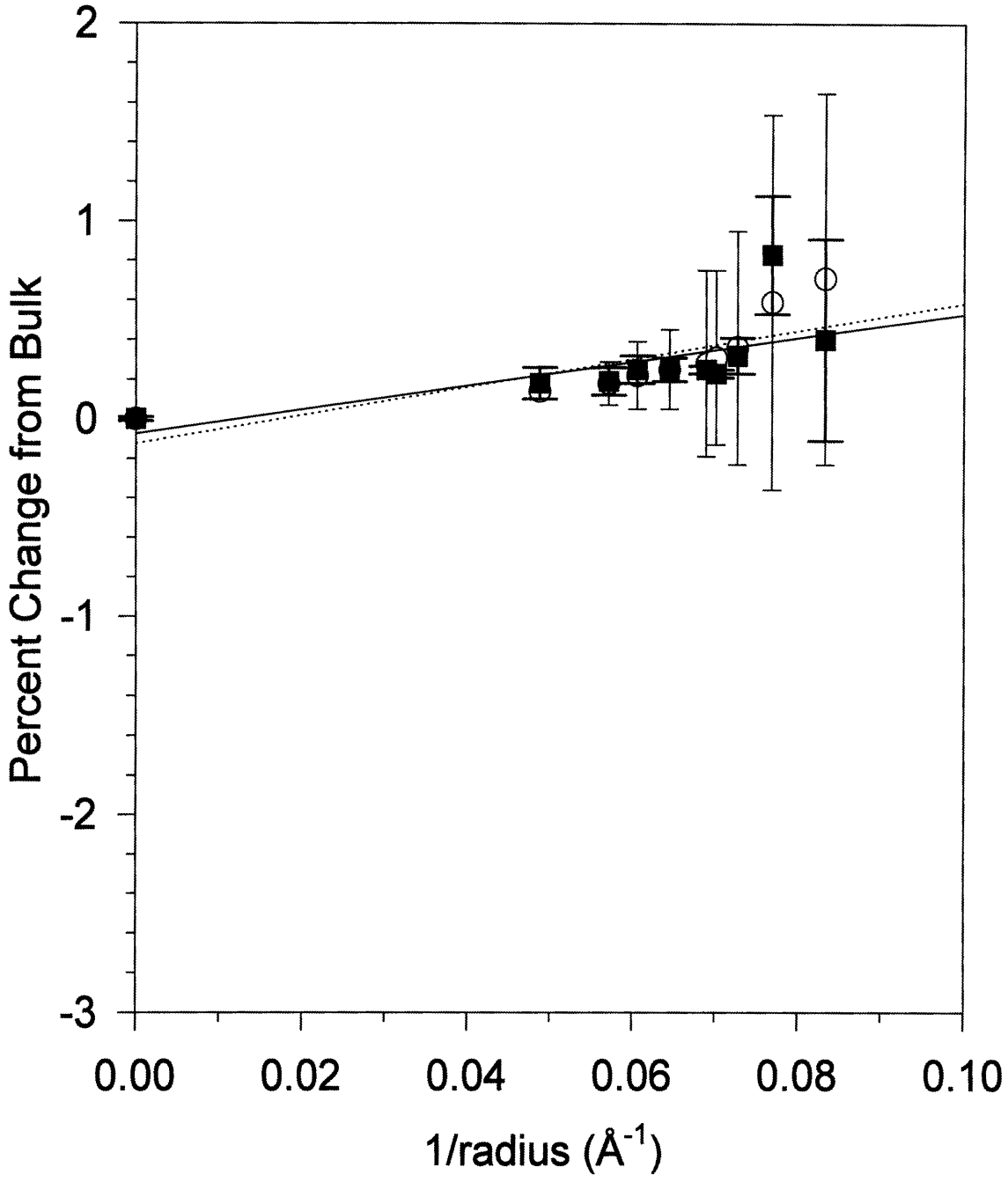

Figure 2-2. Average percent change from the bulk versus 1/radius for simulations fit to three gaussians. Pure wurtzite points are given by ○, with a linear fit given by ·····, while stacking arrangement ...BABACAC... points are given by ■, with a linear fit given by —.

the pure wurtzite series and the series with the stacking faults, with linear fits to the plots for each of the series indicating that the trends are quite similar. Also apparent from Figure 2-2 is the scatter of the shifts, especially predominant for smaller sizes. The scatter is particularly noticeable for clusters of small size with the stacking fault, as the contribution from the {103} reflection is not very intense and therefore difficult to fit with a gaussian. Thus, the use of gaussians to fit the peaks of XRD patterns seems to be a less than desirable method of analysis for smaller particles.

E. Results from Fitting Experimental Patterns with Gaussians

The experimental XRD patterns collected can be seen in Figure 2-3 (page 34). Especially apparent from these patterns is the increasing degree of convolution between the peaks as size decreases. Keeping in mind the difficulties demonstrated above, these experimental patterns were analyzed by fitting with gaussians. A plot of the average shift versus size for these experimental patterns can be seen in Figure 2-4 (page 35). The plot shows little change from that of the bulk, with some scatter present between points. Uncertainties, indicated by the error bars, are mainly due to scatter between shifts for individual peaks in the case of the larger clusters, while difficulties in finding the peaks becomes the major contribution for the smallest clusters. A linear fit to the plot shows a trend virtually independent of size with practically no change from the bulk. Comparison with the analysis of simulations with varying size (Figure 2-2), however, would seem to indicate a slight lattice contraction on the order of a few tenths of a percent from the bulk for this range of particle size.

F. Results from Fitting Experimental Patterns with Simulations

A more straightforward analysis of the experimental patterns was to fit the experimental patterns with a couple of simulated patterns of varying amplitudes, adding a varying linear model of the background scattering, and varying a parameter, r, (the ratio of the experimental d-spacings to the bulk values) that shifts the patterns along the 2θ-

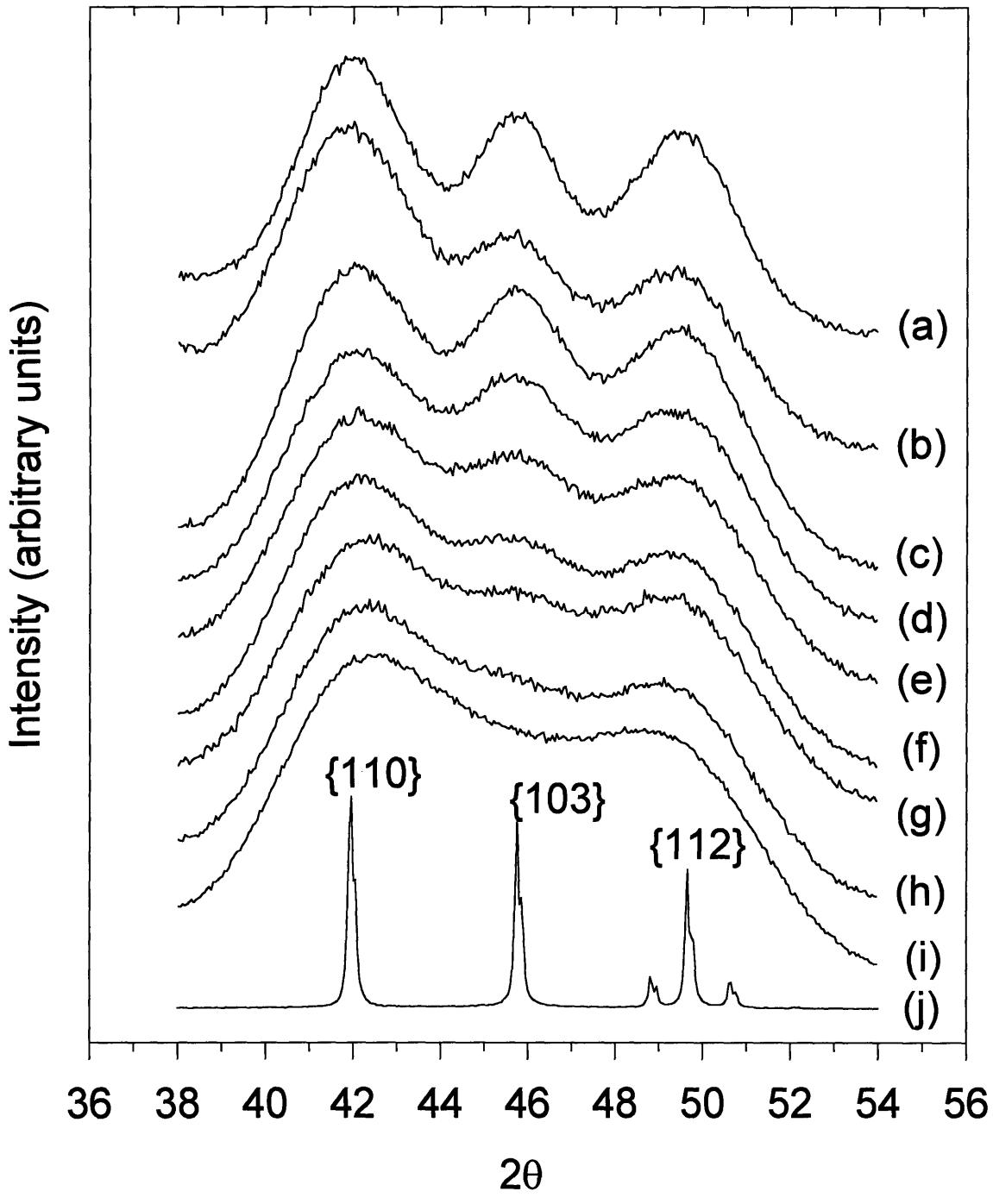

Figure 2-3. Experimental XRD patterns for particles with diameters of (a) 24Å, (b) 26Å, (c) 27.5Å, (d) 28.5Å, (e) 29Å, (f) 31Å, (g) 33Å, (h) 35Å, and (i) 41Å, and for (j) bulk CdSe.

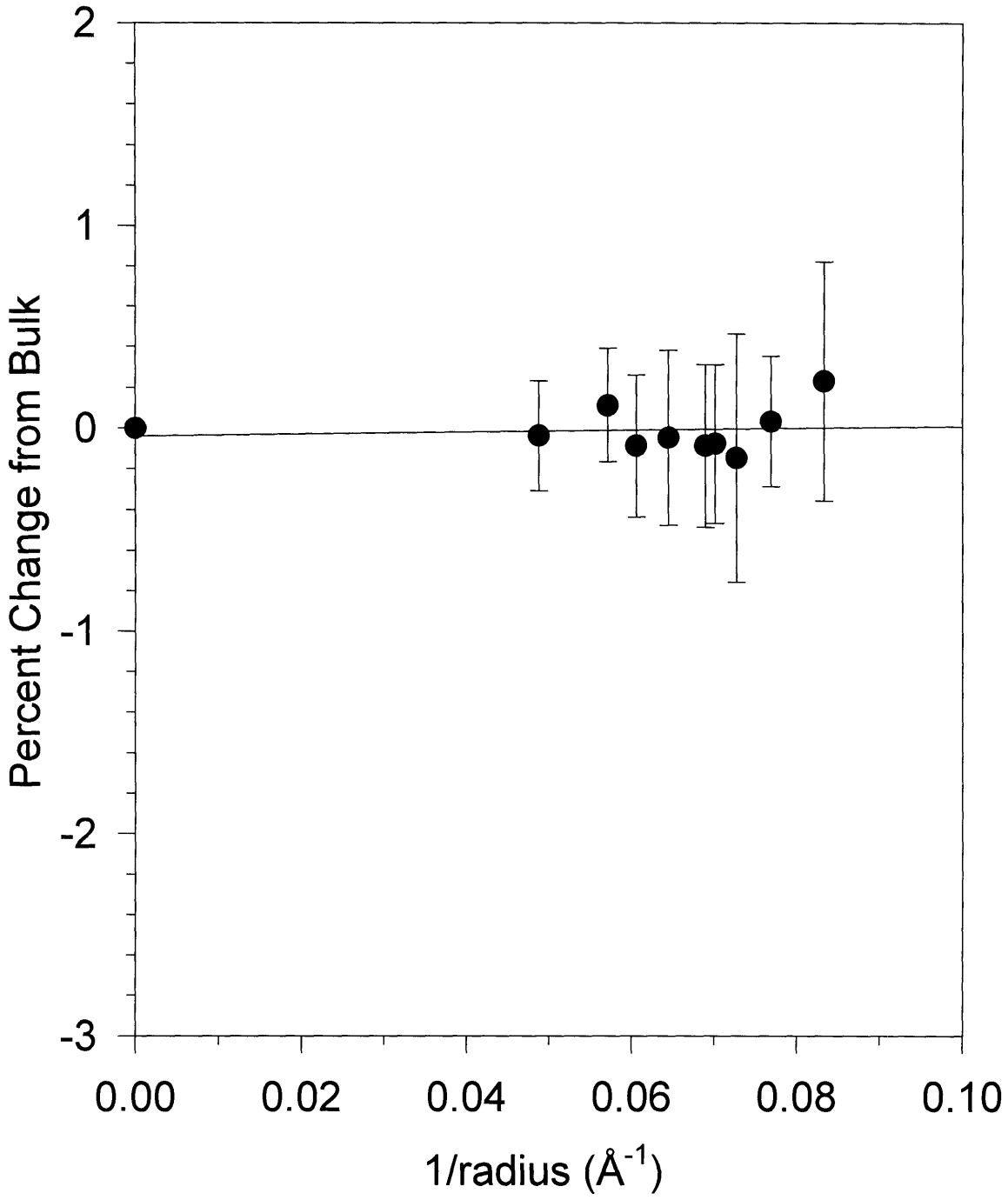

Figure 2-4. Average percent change from the bulk versus 1/radius for experimental XRD patterns fit to three gaussians.

axis. The results of this analysis can be seen in Figure 2-5 (page 37), where percent change in r versus size is plotted. Figure 2-5 shows only a slight contraction from that of the bulk on the order of a few tenths of a percent for this size regime. A linear fit to the plot indicates that there is a trend of increasing contraction as size decreases, though large inherent uncertainties in r detract from the quantitativeness of such a relation. These large uncertainties are due to the fact that r can be varied by large amounts in the fitting procedure with only small changes in the quality of the fit. The fact that the scatter between points is much smaller seems to indicate that these uncertainties are overestimated in the fitting procedure, possibly due to the inability to exactly replicate the experimental patterns. Therefore, though an exact relationship between lattice contraction and particle size cannot be expressed, an upper limit can be put on the lattice contraction for particles in this size range (about 24Å to around 41Å) of about a few tenths of a percent from that of the bulk.

G. Examples of Fits from the Various Methods of Analysis

Figure 2-6 (page 38) shows examples of fits obtained in the various analyses. Figure 2-6a shows two simulations of XRD patterns for particles with 29Å diameter, one pure wurtzite and one with a stacking fault at the center, and fits of these simulations to three gaussians. Figure 2-6b shows the experimental XRD pattern for 29Å diameter particles with a fit to three gaussians. Figure 2-6c shows the fit to the same experimental pattern from Figure 2-6b, but with a fit to the two simulations shown in Figure 2-6a. Both of the fits to experimental patterns include linear models for the background scattering.

V. Conclusion

Analysis of the XRD patterns for semiconductor nanocrystallites presents difficulties due to the small size, ambiguous shape, and defects for such particles. Differences in shape and stacking arrangements cause variations in the observed peak

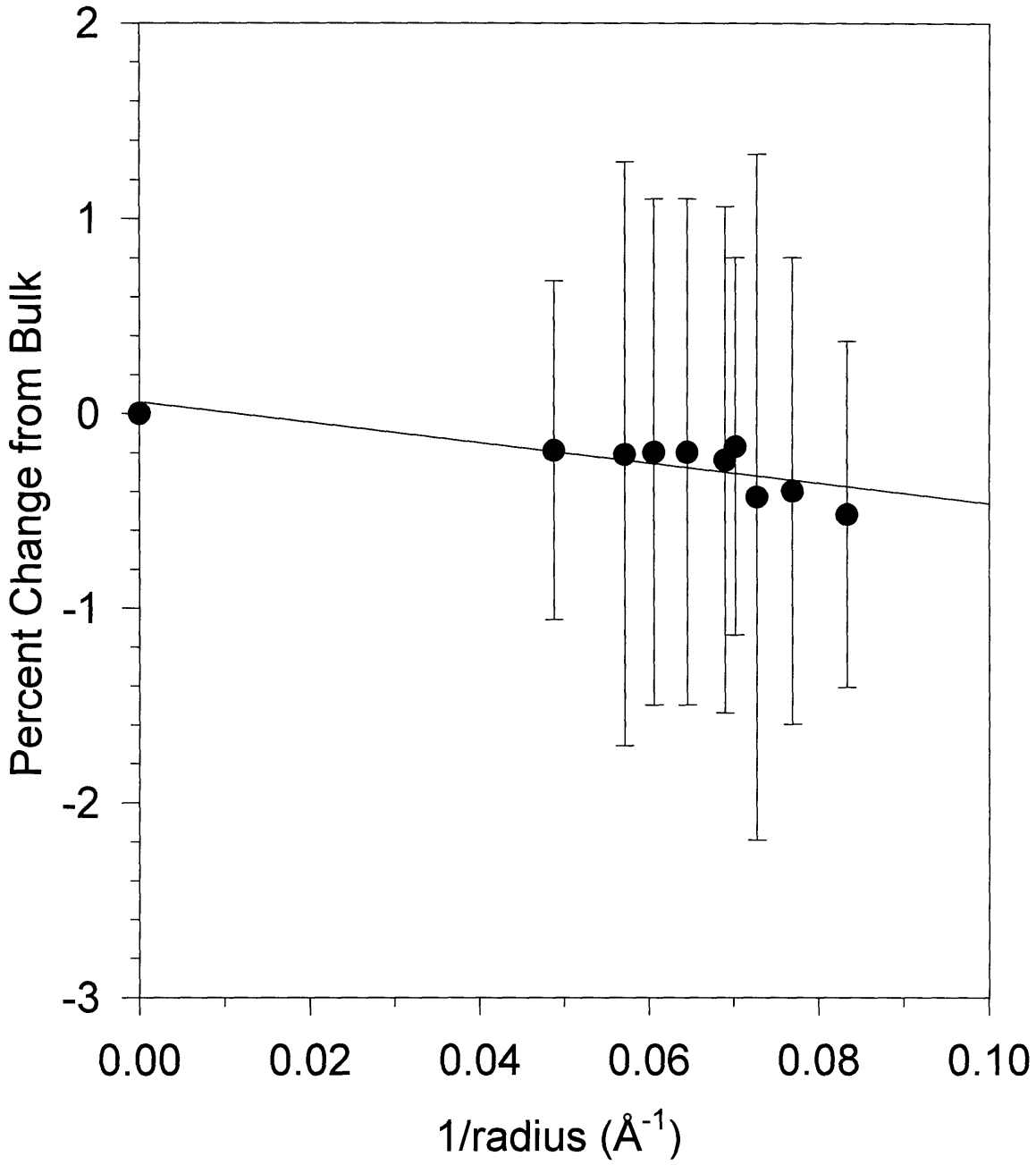

Figure 2-5. Percent change from the bulk versus 1/radius for experimental XRD patterns fit to simulations.

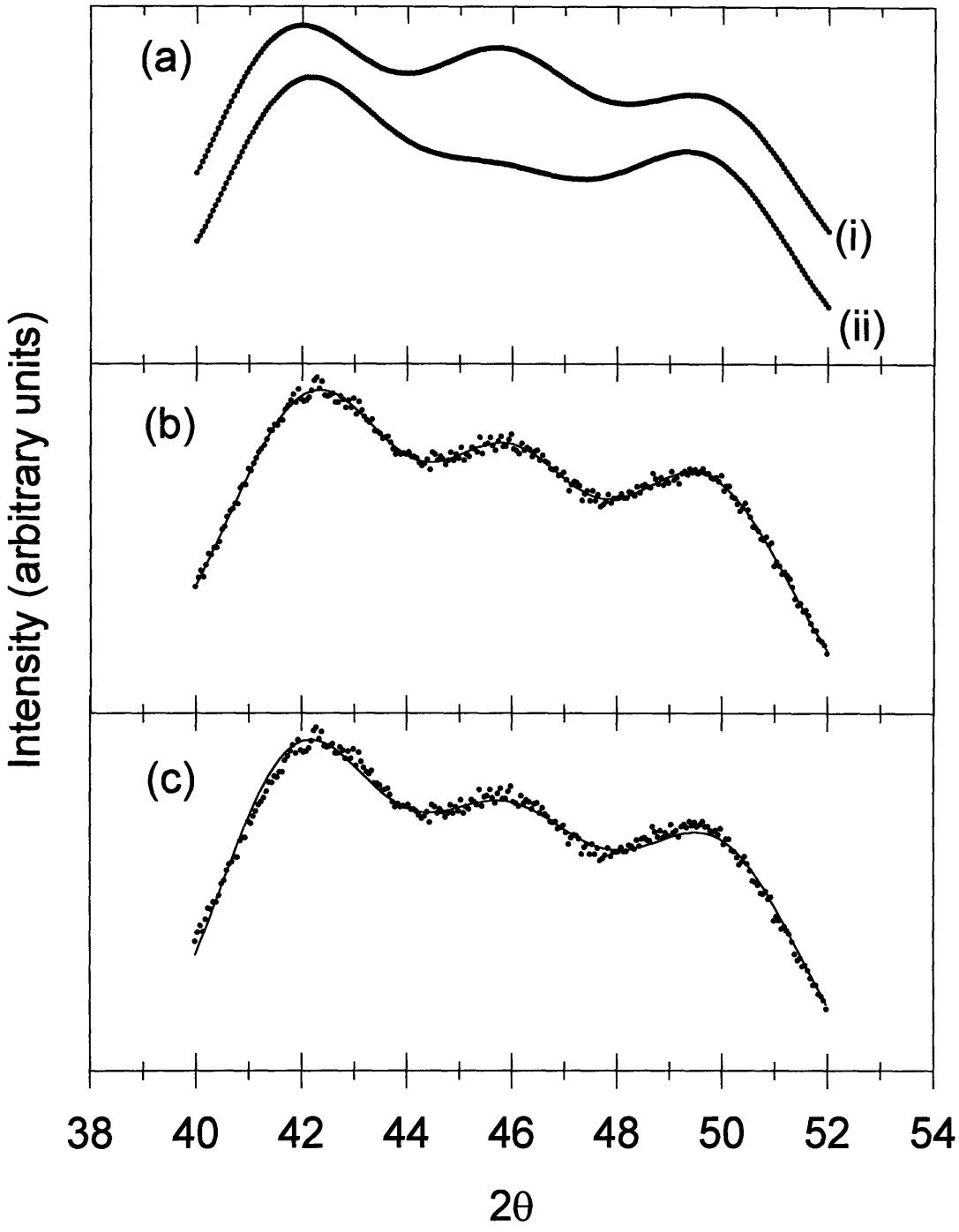

Figure 2-6. Examples of the various analyses performed. (a) Fits for simulations of (i) 29Å dia. particles with pure wurtzite structure and (ii) 29Å particles with the stacking arrangement ...BABACAC... . (b) Fit for experimental pattern of 29Å dia. particles fit to three gaussians. (c) Fit for experimental pattern of 29Å particles fit to the two simulations given in (a). Data points are given by • while fits are indicated by —.

positions. Differences in size also lead to variations in peak positions, as well as to a general trend of a shift of the peaks to lower angles as size decreases, which falsely indicates a slight lattice dilation. Such difficulties lead to the conclusion that direct analysis using the observed peak positions is unreliable, especially when trying to measure small shifts, and such direct analysis in the case of CdSe nanocrystallites shows virtually no change from that in the bulk. A more reliable approach of analysis is to fit experimental data with simulated patterns, along with a modeled background, and shifting the simulated patterns to find the lattice contraction. Such analysis shows a lattice contraction of a few tenths of a percent for CdSe nanocrystallites in the size range of 24Å to 41Å. Large inherent uncertainties are present in these measurements, though such calculations are still useful as upper bounds.

References

(1) Alivisatos, A. P.; Harris, A. L.; Levinos, N. J.; Steigerwald, M. L.; Brus, L. E. *J. Chem. Phys.* **1988**, *89*, 4001.

(2) Bawendi, M. G.; Carroll, P. J.; Wilson, W. L.; Brus, L. E. *J. Chem. Phys.* **1992**, *96*, 946.

(3) Moller, K.; Eddy, C. D.; Stucky, G. D.; Herron, N.; Bein, T. *J. Am. Chem. Soc.* **1989**, *111*, 2564.

(4) Herron, N.; Calabrese, J. C.; Farneth, W. E.; Wang, Y. *Science* **1993**, *259*, 1426.

(5) Krautscheid, H.; Fenske, D.; Baum, G.; Semmelmann, M. *Angew. Chem.* **1993**, *105*, 1364 and *Angew. Chem. Int. Ed. Engl.* **1993**, *32*, 1303.

(6) Vossmeyer, T.; Reck, G.; Kutsikas, L.; Haupt, E. T. K.; Schultz, B.; Weller, H. *Science* **1995**, *267*, 1476.

(7) Cluskey, P. D.; Newport, R. J.; Benfield, R. E.; Gurman, S. J.; Schmid, G. *Mat. Res. Soc. Symp. Proc.* **1992**, *272*, 289.

(8) De Crescenzi, M.; Diociaiuti, M.; Picozzi, P.; Santucci, S. *Phys. Rev. B* **1986**, *34*, 4334.

(9) Balerna, A.; Bernieri, E.; Picozzi, P.; Reale, A.; Santucci, S.; Burattini, E.; Mobilio, S. *Phys. Rev. B* **1985**, *31*, 5058.

(10) Montano, P. A.; Schulze, W.; Tesche, B.; Shenoy, G. K.; Morrison, T. I. *Phys. Rev. B* **1984**, *30*, 672.

(11) Apai, G.; Hamilton, J. F.; Stohr, J.; Thompson, A. *Phys. Rev. Lett.* **1979**, *43*, 165.

(12) Marcus, M. A.; Brus, L. E.; Murray, C.; Bawendi, M. G.; Prasad, A.; Alivisatos, A. P. *nanoStructured Materials* **1992**, *1*, 323.

(13) Murray, C. B.; Norris, D. J.; Bawendi, M. G. *J. Am. Chem. Soc.* **1993**, *115*, 8706.

(14) Bawendi, M. G.; Kortan, A. R.; Steigerwald, M. L.; Brus, L. E. *J. Chem. Phys.* **1989**, *91*, 7282.

(15) Hall, B. D.; Monot, R. *Computers in Physics* **1991**, *5*, 414.

(16) Press, W. H.; Flannery, B. P.; Teukolsky, S. A.; Vetterling, W. T. *Numerical Recipes*, Cambridge University Press: Cambridge, 1986.

(17) Weaver, H. J. *Applications of Discrete and Continuous Fourier Analysis*, Wiley: New York, 1983.

(18) Vetelino, J. F.; Guar, S. P.; Mitra, S. S. *Phys. Rev. B* **1972**, *5*, 2360.

(19) Solliard, C.; Flueli, M. *Surf. Sci.* **1985**, *156*, 487.

(20) Reeber, R. R. *J. Mat. Sci.* **1976**, *11*, 590.